Numerical study of the combustion regimes in naturally-vented compartment fires

Bouaza Lafdal, Racha Djebbar, Pascal Boulet, Rabah Mehaddi, Elmehdi Koutaiba, Tarek Beji, Jose Luis Torero

Fire Safety Journal 131 (2022) 103604

Contents lists available at ScienceDirect

Fire Safety Journal

journal homepage: www.elsevier.com/locate/firesaf

Numerical study of the combustion regimes in naturally-vented compartment fires

Bouaza Lafdal [a,b], Racha Djebbar [a,b], Pascal Boulet [a], Rabah Mehaddi [a,*], ElMehdi Koutaiba [b], Tarek Beji [c], Jose Luis Torero [d]

[a] Université de Lorraine, CNRS, LEMTA, F-54000, Nancy, France
[b] Université Paris-Est, Centre Scientifique et Technique du Bâtiment (CSTB), 84 avenue Jean Jaurès, Champs-sur-marne, 77447, Marne-la-Vallée, France
[c] Department of Structural Engineering and Building Materials, Ghent University, Sint-Pietersnieuwstraat 41, 9000, Ghent, Belgium
[d] Department of Civil, Environmental & Geomatic Engineering, University College London, London, UK

ARTICLE INFO

Keywords:
Under-ventilated
compartment fires
ventilation factor
multi-scale numerical simulations
FDS

ABSTRACT

Numerical simulations are performed to investigate the classical compartment fire problem involving a single door opening. Three different configurations were considered, namely a full-scale (ISO 9705), an intermediate and a small-scale enclosure with various opening heights and widths. A large number of numerical simulations was carried out using the CFD code Fire Dynamics Simulator (FDS)(version 6.7.0). Based on the variation of the average temperature inside the compartment, three combustion regimes were identified namely well-ventilated, transitional and under-ventilated regime. This variation also allowed us to identify the boundaries between regimes. Furthermore, by adopting a non-dimensional representation of the fire heat release rate inside the compartment as a function of the Global Equivalence Ratio (GER), a clear demarcation between these combustion regimes was obtained. A linear correlation has been established between the maximum heat release rate inside the compartment and the ventilation factor. The latter is expressed as $\dot{Q}_{in}^{max} = 850\ A\sqrt{H}$. A linear relation between the maximum air flow rate $\dot{m}_{in}$ and the ventilation factor $A\sqrt{H}$ was found, i.e. $\dot{m}_{in}^{max} = 0.46\ A\sqrt{H}$ where A is the door surface area and H its height.

1. Introduction

In the performance based fire safety engineering approach, the identification of the fire scenario is a crucial step. The scenario depends on several parameters such as the type of activity, the fuel load and the ventilation system. In the case of buildings, one of the characteristic scenarios is a fire in a confined enclosure. Since the sixties, fundamental works on enclosure fires were carried out. In general, during a compartment fire two combustion regimes can be identified. The first one is called well ventilated regime or fuel controlled regime. In this case, the air supply is sufficient to maintain a complete combustion and the products are evacuated easily. On the other hand, this behavior induces an underpressure inside the compartment which favors the inflow of fresh air. The second regime is qualified as under-ventilated, which means that the air supply is not enough to ensure a complete combustion inside the compartment. Usually this regime is reported for small openings. In this case, smoke accumulates on the upper part of the compartment which implies that the mass exchange is dominated by hydrostatic pressure at the opening. Under this regime, and by considering Bernoulli's equation, the inlet air flow rate can be expressed as $\dot{m}_{in} = CA\sqrt{H}\ (kg/s)$, where $A\sqrt{H}$ is the ventilation factor introduced for the first time by Kawagoe [1] one of the pioneer researchers on this topic. Here A is the opening area and H its height. Babrauskas [2] estimated the constant C and expressed the air flow entering a compartment as $\dot{m}_{in} = 0.5\ A\sqrt{H}$. By using the expression of the inlet air flowrate and assuming that the total amount of oxygen entering in the enclosure is involved in the combustion, the maximum heat release rate inside the compartment can be expressed as:

$$\dot{Q}_{in}^{max} = 0.23 \times \Delta H_{c_{O_2}} \times C \times A\sqrt{H}\ (kW), \tag{1}$$

where 0.23 is the oxygen mass fraction in the air, C is a flow coefficient ($C = 0.5$), $A\sqrt{H}$ is the ventilation factor and $\Delta H_{c_{O_2}}$ the heat of combustion per mass of oxygen consumed (13.1 MJ/kg). This value was recommended by Huggett [3] based on an experimental investigation

* Corresponding author.
E-mail address: rabah.mehaddi@univ-lorraine.fr (R. Mehaddi).

https://doi.org/10.1016/j.firesaf.2022.103604
Received 20 August 2021; Received in revised form 2 May 2022; Accepted 4 May 2022
Available online 12 May 2022
0379-7112/

Nomenclature

ΔH_{co_2}	Heat of combustion per mass of oxygen consumed [MJ/kg]
$\dot{Q}$	Heat release rate [kW]
Φ	Global Equivalence Ratio (GER) [−]
ρ	Density [kg/m^3]
A	Opening area [m^2]
$C_{DEARDORFF}$	Deardorff coefficient [−]
C_p	Specific heat capacity [kJ/(kg.K)]
H	Opening height [m]
K	Thermal conductivity [W/m/K]
W	Opening width [m]
ΔH_c	Heat of combustion [kJ/kg]
$\dot{m}_f$	Fuel flow rate [kg/s]
$\dot{m}_{in}$	Inlet air flow [kg/s]
$\dot{Q}_{in}$	HRR inside the compartment [kW]
$\tau_{chemical}$	Characteristic chemical time scale [s]
$\tau_{mixixng}$	Characteristic mixing time scale [s]
P	Prescribed heat release rate [kW]
s	Stoichiometric fuel to oxygen ratio [−]
D^*	Characteristic fire diameter [−]
g	Gravity acceleration [m/s^2]
T_0	Ambient temperature [K]

involving a wide range of fuels, including organic liquids and gases, natural fuels and synthetic polymers. This value of (13.1 MJ/kg) is accurate up to ± 5%. Quintiere et al. [4] estimated the maximum heat release rate inside a compartment as $\dot{Q}_{in}^{max} = 1500\ A\sqrt{H}(kW)$. This is only valid under the assumptions listed above. An extensive review of the compartment framework was presented by Torero et al. [5] and Majdalani [6]. Despite the strong assumptions that have allowed to express the heat release rate inside the compartment ($\dot{Q}_{in}^{max} = 1500\ A\sqrt{H}\,(kW)$), this formulation is systematically used and, sometimes, beyond its application range.

During the last decades, numerous experimental studies have been carried out on compartment fires. Different combustion regimes were identified. Takeda and Akita [7] explored the effect of the ventilation factor on the combustion regime. They recorded four combustion regimes in the case of compartment fire with a liquid pool fire. In the first regime ($A\sqrt{H} < 0.09 \times 10^{-2}(m^{(5/2)})$), the air supply through the opening was not sufficient. As consequence, the fire extinguishes due to the lack of oxygen. The second regime ($0.09 \times 10^{-2}(m^{(5/2)}) < A\sqrt{H} < 0.23 \times 10^{-2}(m^{(5/2)})$) corresponds to a laminar combustion controlled by the amount of oxygen entering through the openings. The third one is characterized by unstable and oscillating flames. In the last regime ($0.78 \times 10^{-2}(m^{(5/2)}) < A\sqrt{H} < 2.8 \times 10^{-2}(m^{(5/2)})$), the size of the opening was sufficient to allow a perfectly ventilated fire controlled by the quantity of fuel available. A similar behavior was observed by Tewarson [8], Kim et al. [9], Utiskul et al. [10] during pool fires. Snegirev et al. [11] conducted a small-scale experimental study on compartment fires using a propane burner as a fire source. Three combustion regimes were observed. In the first one, combustion occurs only inside the compartment. This represents the well-ventilated regime. The second regime is characterized by flames appearing outside the enclosure. Finally, for the third regime, only external combustion was observed. A similar behavior was also reported by Lock et al. [12] during their full-scale experimental study with a gas burner. Recently, Ren et al. [13] investigated experimentally the transitional behavior of under-ventilated compartment fires. In this study, the fire source also consisted of a gas burner. These authors also reported the same three combustion regimes. Note that there is an important difference between liquid and gaseous fuels regarding the flow regimes identified by the authors. The oscillatory regime was only observed for liquid pool fires and this can be linked to the importance of the heat feedback from the surrounding environment to the liquid surface and subsequent evaporation. However, when there is no more oxygen in the environment, pool fires undergo extinction, while the fire issuing from a gas burner burns completely outside the compartment.

Most of the empirical correlations have been developed based on small-scale experiments. A relevant question to ask here is whether these correlations remain valid at full-scale. This issue has been raised since the beginnings of fire safety science. Earlier works by Heskestad [14], Quintiere [15], Quintiere et al. [16], Quintiere [17] and Emori and Saito [18] provided the first successful scaling results. These authors and others highlighted the importance of the choice of the scaling variables, because it is not possible to preserve all the variables at the same time.

Nowadays, with the increase of the numerical calculation capacities and the significant development of Computational Fluid Dynamics (CFD), numerical simulation becomes an attractive alternative to experimental studies. For instance, Suard et al. [19] obtained a good agreement between the CFD model ISIS and the experimental results in the case of a small-scale enclosure fire. Zhao et al. [20] investigated under-ventilated compartment fires with external flames using Fire Dynamics Simulator (FDS). They found a linear relationship between the ventilation factor and the heat release rate inside the compartment. This relation reads as $\dot{Q}_{in} = 1130.7\ A\sqrt{H}(kW)$. The proportionality coefficient is different from the one obtained by Babrauskas [2]. According to Zhao et al., the discrepancy can be explained by the fact that the oxygen entering the compartement is not completely used during the combustion. A similar difference has been observed for the inlet air flow ($\dot{m}_{in} = 0.41\ A\sqrt{H}$). A similar relationship was found by Asimakopoulou et al. [21] for the fire heat release rate with a different coefficient of proportionality namely $\dot{Q}_{in} = 925\ A\sqrt{H}(kW)$.

The studies mentioned above and others highlighted a very important aspect of compartment fires, which is the existence of several combustion regimes. However, to our knowledge, there is no clear criterion for separating these different regimes. Many authors use the theoretical relationship $\dot{Q}_{in} = 1500\ A\sqrt{H}(kW)$ to discriminate between under-ventilated and well-ventilated regimes. However, this demarcation is only theoretical. Experimental studies rely on temperature measurements to determine the transition to the under-ventilated regime [13,22]. Other authors use visual criteria such as the appearance of flames outside the compartment or quantitative criteria such as the onset of CO production, which indicates a lack of oxygen. The main difficulty is that all these studies do not provide a universally accepted criterion. In this study, a comprehensive analysis is carried out in an attempt to clarify some aspects related to combustion regimes in enclosure fires and, more particularly, determine a clearer global criterion for the onset of under-ventilated combustion. Another issue is the determination of the boundary between the transient regime (combustion inside and outside the compartment) and the fully under-ventilated regime (combustion entirely outside the compartment).

In the present work, a numerical analysis is carried out using the CFD code FDS in order to investigate under-ventilated enclosure fires. More than 300 simulations were performed, in which different scales, opening geometries and heat release rates were considered. This paper is organized as follows. In §2, the numerical configurations are presented. In §3, the numerical results are presented and discussed. Finally, our conclusions are drawn in §4.

2. Numerical set-up

The CFD code Fire Dynamics Simulator (FDS) was developed by the National Institute of Standards and Technology (NIST) [23]. This code uses the low Mach number assumption to solve the momentum, continuity and energy equations. Turbulence is modeled using large-eddy simulation (LES) which means that large eddy structures are solved, while the small ones are predicted using subgrid-scale model. More particularly, in our case, the modified Deardorff model (default model in FDS) is used with a constant $C_{DEARDORFF} = 0.1$. The combustion is assumed as infinitely fast based on the mixing-limited model [24]. The radiation transport equation was modeled using a Finite Volume Method (FVM) with 100 discrete angles, under the gray gas absorption assumption. For this study all models by default in FDS have been used, unless specified otherwise. As mentioned previously, full-scale, intermediate and small-scale configurations are studied (see Fig. 1). The simulation conditions and dimensions are given in Table 1.

FDS is well documented and validated against numerous experimental studies as reported by McGrattan et al. [25]. Hwang et al. [26] performed numerical simulations using FDS (version 5.1.6) to investigate the full-scale ISO 9705 compartment fire. These authors explored both well-ventilated and under-ventilated conditions. The numerical results were compared to the experimental study by Lock et al. [27]. The comparison between the numerical and experimental results showed that FDS predictions were in a good agreement with the experimental results for both temperature and species. Pikiokos [28] numerically investigated the flow characteristics at the opening. In this study Pikiokos used FDS (version 6.3.2.) to simulate the full-scale ISO 9705 compartment fire conducted by Bryant [29–31]. The doorway temperature and velocity profiles predicted by FDS were compared to the experimental results. In general, a satisfactory agreement was found between the numerical and experimental results, with an error of 4.19% for temperature and from 8% to 32% for velocity depending on the considered position. Moinuddin et al. [32] also performed an experimental and numerical study of large-scale compartment fires in an ISO 9705 compartment with steel walls. FDS (version 5.3.1) was used for the numerical modeling. A satisfactory agreement was observed between the temperatures predicted by FDS and the experimental results. Although it should be noted that in some cases lower temperatures were predicted, this difference was explained by the large amount of heat escaping through the door. As it was shown by these different validation studies, FDS simulations of ISO 9705 are generally in a good agreement with the experimental work, especially for the temperature measurements. For this reason, in the present study, full-scale simulations were carried out using an ISO-9705 compartment with the following properties: thickness 2.5 cm, density $\rho = 1440$ (kg/m^3), conductivity $K = 0.48$ ($W/m/K$), specific heat capacity $C_p = 840$ ($J/kg/K$). For this configuration, a 0.96 m square hexane (C_6H_{14}) burner was considered as a fire source. The burner is located at 0.42 m above the ground.

The intermediate scale and small-scale configuration are made of 5 cm thick calcium silicate boards with the following characteristics: density $\rho = 2900$ (kg/m^3), conductivity $K = 0.22$ ($W/m/K$), specific heat capacity $C_p = 970$ ($J/kg/K$). The fire source is a propane burner of dimensions 0.4 m × 0.4 m placed in the center of the compartment. The simulation duration was fixed to 120 s for the small and intermediate scale and 150 s for the full-scale.

Temperatures are evaluated at five different positions, four of them are located inside the compartment at each corner and the fifth one located at the doorway symmetry plan (see Fig. 2). The use of numerical simulations offers the possibility to directly evaluate a wide range of variables, such as the inlet and outlet flowrate and even more complex quantities like the heat release rate within predefined volumes.

In order to obtain accurate simulations, a sensitivity analysis was conducted to make sure that the mesh size is suitable for this study. The results are shown in appendix A. For the present study it was found that a uniform mesh size of 2 cm was sufficient to reach convergence.

On the other hand, McGrattan et al. [33] suggested that the grid size should be equal or less to 0.1 D^* with $D^* = \left(\frac{\dot{Q}}{\rho_0 C_p T_0 \sqrt{g}}\right)^{2/5}$ representing the characteristic fire diameter. This suggestion was confirmed by Merci and Van Maele [34]. In our study the fire heat release rate ranged between 25 kW and 3500 kW which means that D^* varies between 0.22 m and 1.58 m, leading to an optimal mesh size (0.1 D^*) ranging between 2.2 cm and 15.8 cm, which supports the results obtained with the mesh sensitivity analysis.

Flame extinction is a very important aspect in the study of compartment fires in particular. To deal with these phenomena, FDS includes an extinction model based on the critical flame temperature concept. Indeed, extinction occurs if the combustion in a computational cell would not raise the temperature of the mixture above the critical flame temperature. This criterion is expressed as an inequality as follows [24,35].

$$Z_F^0 h_F(T) + \widetilde{\varphi} Z_f^0 h_A(T) + \widetilde{\varphi} Z_P^0 h_P(T) < Z_F^0 h_F(T_{CFT}) + \left[(\widetilde{\varphi} - 1) Z_P^0 + Z_P\right] h_P(T_{CFT}), \quad (2)$$

where T_{CFT} is the critical flame temperature, T is the pre-reaction temperature, Z_F^0, Z_A^0 and Z_P^0 are respectively the mass fractions of Fuel, Air and Products at the beginning and Z_F, Z_A and Z_P the mass fraction at the end and $\widetilde{\varphi}$ is a modified equivalence ratio, defined as

$$\widetilde{\varphi} = \frac{Z_A^0 - Z_A}{Z_A^0}, \quad (3)$$

In order to evaluate the inequality (2), it is necessary to determine the critical flame temperature T_{CFT}. The latter is evaluated based on the limiting oxygen fraction as follows

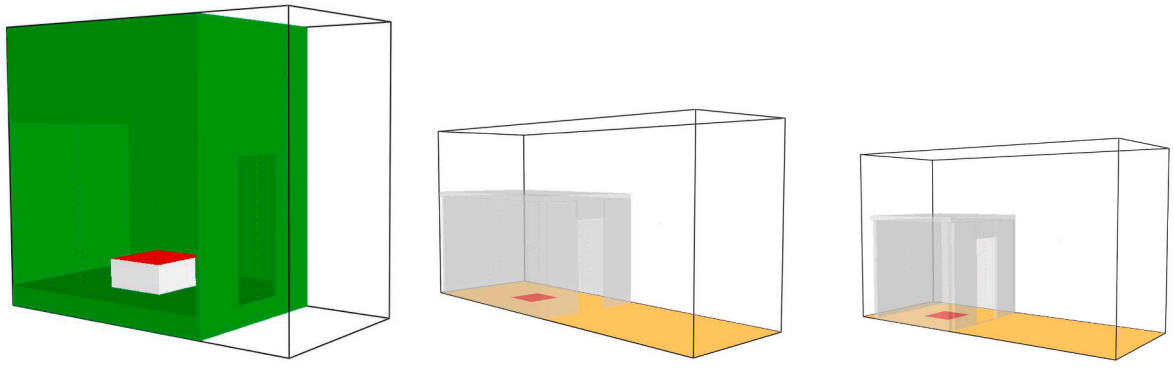

Fig. 1. Compartment configurations, (a) full-scale ISO9705, (b) intermediate scale and (c) small-scale (Smokeview).

Table 1
Summary of the simulations parameters.

Configuration	Dimensions (m^3)	Heat release rate (kW)	Opening dimensions (m)		Ventilation factor $A\sqrt{H}$ ($m^{5/2}$)	Number of simulations
			W (m)	H (m)		
Small-scale	1.2 × 1.2 × 1.2	25–350	0.4	0.5	0.1414	12
			0.4	1	0.4	12
			0.6	1	0.6	12
Intermediate scale	2 × 1.2 × 1.2	25–3500	0.4	1	0.4	27
			0.6	1	0.6	27
			0.8	1	0.8	27
			0.8	0.6	0.3718	27
Full-scale ISO 9705	3.6 × 2.4 × 2.4	500–11500	0.36	1.75	0.83	12
			0.6	1.86	1.52	12
			0.84	1.98	2.34	12
			1.08	2.1	3.29	12
			1.32	2.22	4.37	12
			5.58	2.34	5.58	12

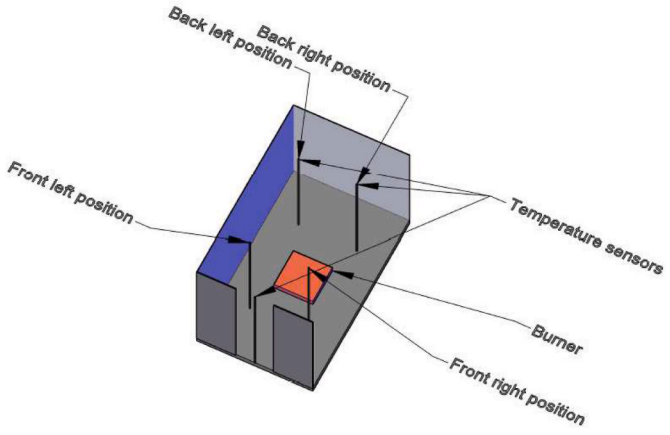

Fig. 2. Sketch of the numerical configuration.

$$T_{CFT} = T_0 + Y_{O_2}^{lim}\frac{\Delta H_c/s}{\overline{C_p}}, \tag{4}$$

where $Y_{O_2}^{lim}$ represents the limiting oxygen fraction, $\overline{C_p}(kJ/(mol\,K))$ is the average heat capacity, $\Delta H_c(kJ/kg)$ is the heat of combustion, s is the stoichiometric fuel to oxygen ratio and T_0 is the initial temperature of the environment. It is also assumed that the excess fuel will be treated as diluent but not the excess of the air. In other words, combustion would be possible in a cell with small quantity of fuel and excess of air but not in a cell with small amount of air and excess of fuel. This seems to be reasonable in the case of a compartment fire. As it can be noticed, the unique way to control the extinction is by modifying the limiting oxygen concentration. This is discussed in section 3.3.

3. Results and discussion

In this section we present the results of the parametric study in which heat release rate, ventilation factor and compartment size were varied. The delimitations of the different combustion regimes are highlighted.

3.1. Air flow rate

The amount of air entering through the openings is a very important parameter in the evolution of a compartment fire. In the present simulations, the inlet and outlet air flow rate are obtained by integrating the mass flux through the door. It can be obtained directly using a specific device. A typical variation of the inlet mass air flow is shown in Fig. 3a ($A\sqrt{H} = 0.3718\ m^{5/2}$, $P = 200$ kW). For each configuration (ventilation factor, prescribed heat release rate) the average value through the steady state is determined as illustrated by the blue line in Fig. 3a. These mean values are presented in Fig. 3b as a function of the prescribed heat release rate P. This allowed us to determine the maximum inlet mass flow rate for each ventilation factor, see Fig. 3c. The superscript "max" refers to this maximum value of $\dot{m}_{in}$.

In the case of a compartment fire, the maximum inlet air flow is generally expressed as $\dot{m}_{in} = 0.5\,A\sqrt{H}$. This formulation is based on the assumption that the fuel flow is negligible compared to the air flow entering the room ($\dot{m}_{in} \gg \dot{m}_f$). In a recent study, Delichatsios et al. [36] demonstrated that the inlet mass flow rate can be expressed as $\dot{m}_{in} = 0.5A\sqrt{H} - 0.53\dot{m}_f$ (where $\dot{m}_f$ is the fuel flow rate).

In Fig. 3c, the maximum inlet air flow is plotted as a function of the ventilation factor $A\sqrt{H}$ and compared to the theoretical relation by Babrauskas [2] and Delichatsios et al. [36]. As it can be seen, the linear relationship between the maximum inlet air flow and the ventilation factor seems to be well respected. Equation $\dot{m}_{in} = 0.46\,A\sqrt{H}$ is represented by the red line. The simulations results showed also a good agreement with the correlation proposed by Delichatsios et al. [36] as it is shown by the green line in Fig. 3c.

3.2. Combustion regimes

Since this study deals with various scale simulations, this gives us the possibility to investigate the scaling problem. For this purpose, a dimensionless representation was chosen to allow comparison between the different cases. The first dimensionless parameter is the Global Equivalence Ratio (GER) Φ, introduced by Babrauskas et al. [37]. It is defined as

$$\Phi = \frac{s\dot{m}_f}{\dot{m}_{O_2}}, \tag{5}$$

where s is the stoichiometric fuel/oxygen ratio and $\dot{m}_f$, $\dot{m}_{O_2}$ are the prescribed fuel mass flow rate and the oxygen mass flow rate entering the enclosure respectively. According to this definition we can distinguish two combustion regimes, an over-ventilated regime for $\Phi < 1$ and an under-ventilated regime for $\Phi > 1$. The second key parameter in this study is the heat release rate inside the compartment, hereafter referred to as $\dot{Q}_{in}$. The latter is evaluated by integrating the heat release rate per unite volume over the specified domain, in this case the inside of the compartment. Then, the mean value during the steady state period is considered. This quantity is compared to the prescribed heat release rate (theoretical heat release rate P).

Fig. 4 presents the variation of the ratio $\dot{Q}_{in}/P$ versus the Global Equivalence Ratio (GER) Φ for the different scales and ventilation factors. Based on this representation ($\dot{Q}_{in}/P = f(\Phi)$), we may distinguish three combustion regimes. The first regime, i.e., well-ventilated regime, corresponds to $\dot{Q}_{in}/P = 1$. During this regime, the reaction is held

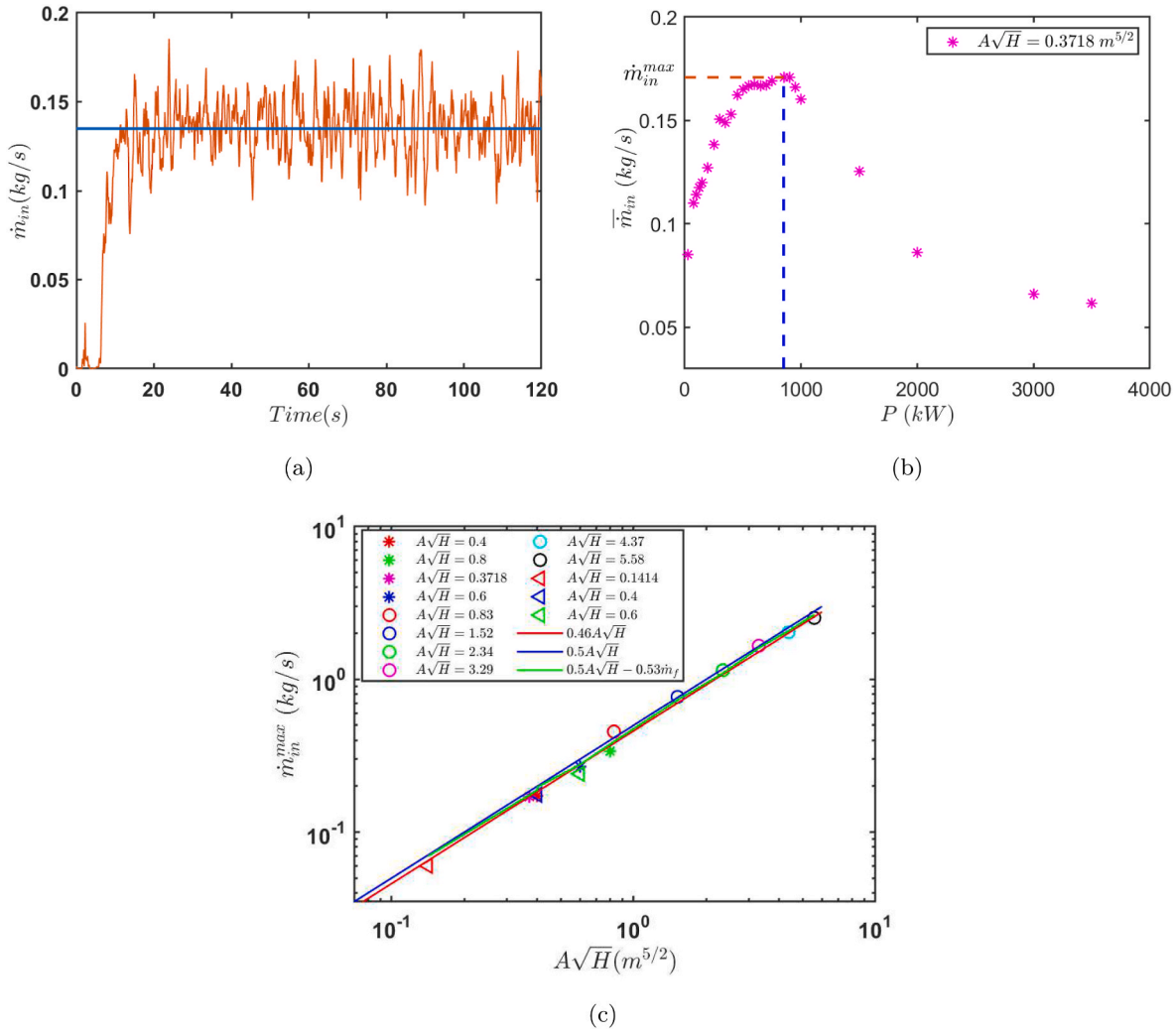

Fig. 3. (a) Typical variation of the inlet air flow (intermediate scale, $A\sqrt{H} = 0.3718\ m^{5/2}$, $P = 200$ kW), (b) variation of the mean inlet air flow as a function of the prescribed heat release rate for a ventilation factor of 0.3718 $m^{5/2}$. (c) Variation of the maximum inlet air flow versus the ventilation factor: ∘ full-scale (500 kW ≤ P ≤ 11500 kW), * intermediate scale (25 kW ≤ P ≤ 3500 kW), ◁ small-scale (25 kW ≤ P ≤ 350 kW).

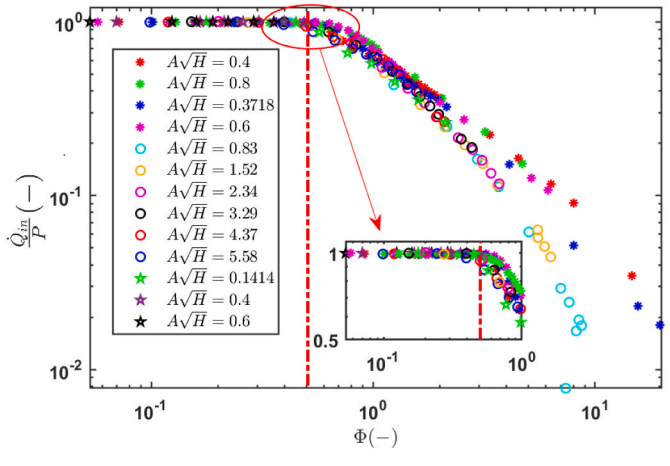

Fig. 4. Variation of the ratio $\dot{Q}_{in}/P$ versus the Global Equivalence Ratio (∘ full-scale, * intermediate scale and ⋆ small-scale), the dashed line represents the delimitation between the well-ventilated and the under-ventilated regime.

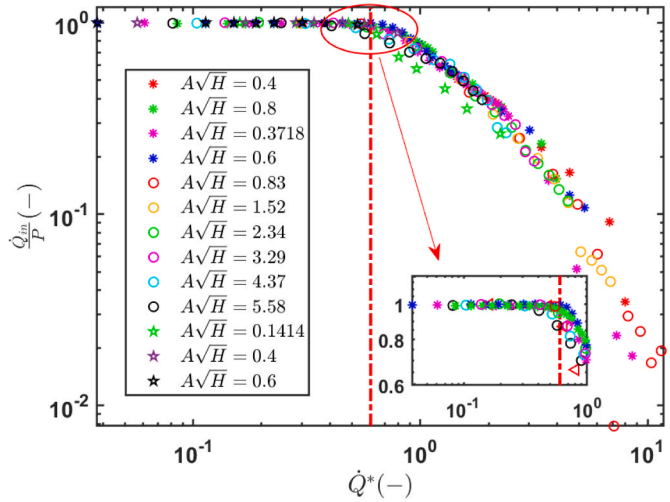

Fig. 5. Variation of the ratio $\dot{Q}_{in}/P$ versus dimensionless heat release rate (∘ full-scale, * intermediate scale and ⋆ small-scale).

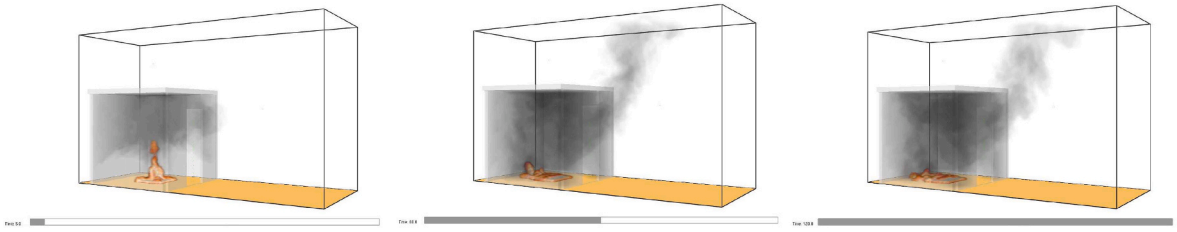

Fig. 6. Well-ventilated combustion regime(1st regime): the flame is within the compartment (small-scale, $A\sqrt{H} = 0.4(m^{5/2})$, $HRR = 25$ kW).

exclusively within the enclosure. An illustration of this regime is shown in Fig. 6 for a small-scale simulation with an HRR of 25 kW and $A\sqrt{H} = 0.4\ (m^{5/2})$. As it can be seen, the flames are exclusively within the compartment.

However, when the GER Φ rises, the under-ventilated conditions start to appear, which is characterized by external flames indicating that the fuel burns outside as can be seen in Fig. 7. The transition occurs when the Global Equivalence Ratio reaches a value of 0.5 as indicated by a red dashed line in Fig. 4. This same critical value ($\Phi > 0.5$) was identified earlier by Babrauskas et al. [37] and Pitts [38]. They reported an increase in the concentration of CO, which is the first indicator of incomplete combustion. Finally, for the highest values of Φ we can notice that the ratio $\dot{Q}_{in}/P$ is almost equal to zero. This reflects the fact that the major part of the combustion is taking place outside the compartment (see Fig. 8). This dimensionless analysis can be also performed using a dimensionless heat release rate defined as

$$\dot{Q}^* = \frac{P}{\rho_0 C_p T_0 \sqrt{g} l^{5/2}}, \tag{6}$$

where P is the prescribed heat release rate, ρ_0 is the ambient air density, C_p is the specific heat capacity of air, T_0 is the ambient temperature, g is the gravity acceleration and l is a characteristic length. In order to include the ventilation factor which is a very important parameter, we took $l^{5/2} = A\sqrt{H}$. This dimensionless heat release rate is known as the Zukoski number [39] and it represents the ratio between the heat release rate of the fire and the advected enthalpy rate [17]. Fig. 5 presents the variation of the ratio $\dot{Q}_{in}/P$ versus the dimensionless heat release rate $\dot{Q}^*$ for the different scales and ventilation factors.

Note that, according to this formulation ($\dot{Q}_{in}/P = f(\dot{Q}^*)$), it is possible to give a demarcation based on the geometrical characteristics of the compartment opening as well as the prescribed HRR (P) which can be very useful in engineering because once we estimate the fire load in a compartment, one can determine the evolution of a fire and whether it may become under-ventilated or not. The criterion

$$\dot{Q}^* = \frac{P}{(\rho_0 C_p T_0 \sqrt{g} A\sqrt{H})} = 0.6, \tag{7}$$

marks the boundary between the well-ventilated (combustion only inside the compartment) and the under-ventilated regimes (appearance of external flames). Furthermore, for $\dot{Q}^* = 0.6$ we still have $P = \dot{Q}_{in}$, and thus we define a critical value for $\dot{Q}_{in}$ as follows

$$\dot{Q}_{in}^{cri} = 0.6 \times \rho_0 C_p T_0 \sqrt{g} A\sqrt{H} = 660\ A\sqrt{H}(kW), \tag{8}$$

with $\rho_0 = 1.2(kg/m^3)$, $C_p = 1(kJ/kg.K)$, $T_0 = 293(K)$, $g = 9.81(m.s^{-1})$. Beside the combustion regimes, we can observe that for the well-ventilated conditions adapting a dimensionless representation using both $\dot{Q}^*$ and GER (Φ) we can overcome the scale effect and all the points are on the same curve. However, for the under-ventilated regime, a small gap can be seen between the intermediate and full-scale especially in the case of scaling with Φ. This gap is less important when considering $\dot{Q}^*$. This is mainly due to the scale difference.

The analysis of the variation of the average temperature (spatial and temporal mean temperature over all the thermocouples) inside the compartment confirms the observation of different regimes and gives us more details about their characteristics. Fig. 9a and Fig. 9b present a typical variation of the average temperature inside the compartment versus the Global Equivalence Ratio. The variation of the average temperature inside the compartment is also represented as a function of the dimensionless heat release rate Fig. 9c and Fig. 9d. We can identify three trends. The first one (R1) where the temperature inside the enclosure increases, represents the well-ventilated regime (the combustion is held inside the compartment). In the second case (R2), the temperature is almost steady. This marks the beginning of the under-ventilated regime. The combustion occurs both inside and outside the enclosure (transitional regime). Finally, the third regime (R3) is also an under-ventilated regime which is characterized by a sudden drop in the temperature reaching its lowest level.

This behavior reflects the fact that the combustion is mainly taking place outside the compartment. This third regime is highly dependent on the extinction model, once the extinction condition is no longer fulfilled inside the compartment the fire leaves the compartment and takes place outside. The delimitation of the different combustion regimes based on the evolution of the temperature is a very common technique among experimentalists, since it is not possible to measure the heat release rate inside a compartment. From the present data, we can determine the

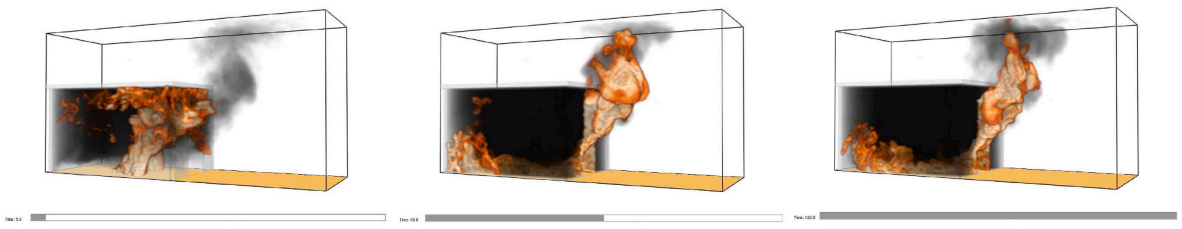

Fig. 7. Under-ventilated combustion regime(2^{nd} regime): the reaction is held inside and outside the enclosure (intermediate scale, $A\sqrt{H} = 0.4(m^{5/2})$, $HRR = 600$ kW).

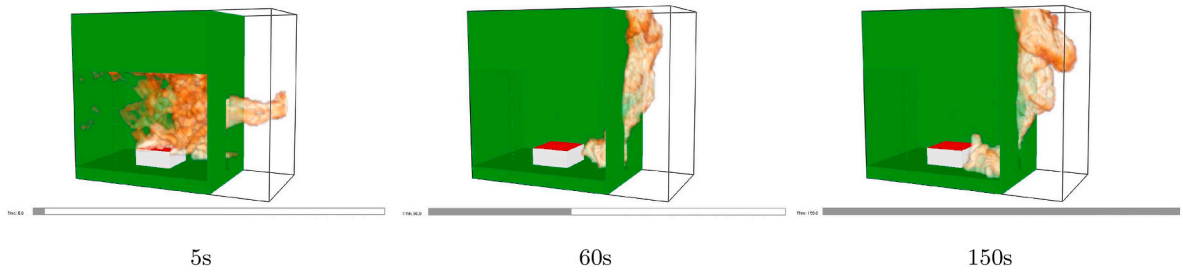

Fig. 8. Under-ventilated combustion regime(3^{rd} regime): the major part of the combustion takes place outside the compartment (full-scale, $A\sqrt{H} = 0.83(m^{5/2})$, $HRR = 3500$ kW).

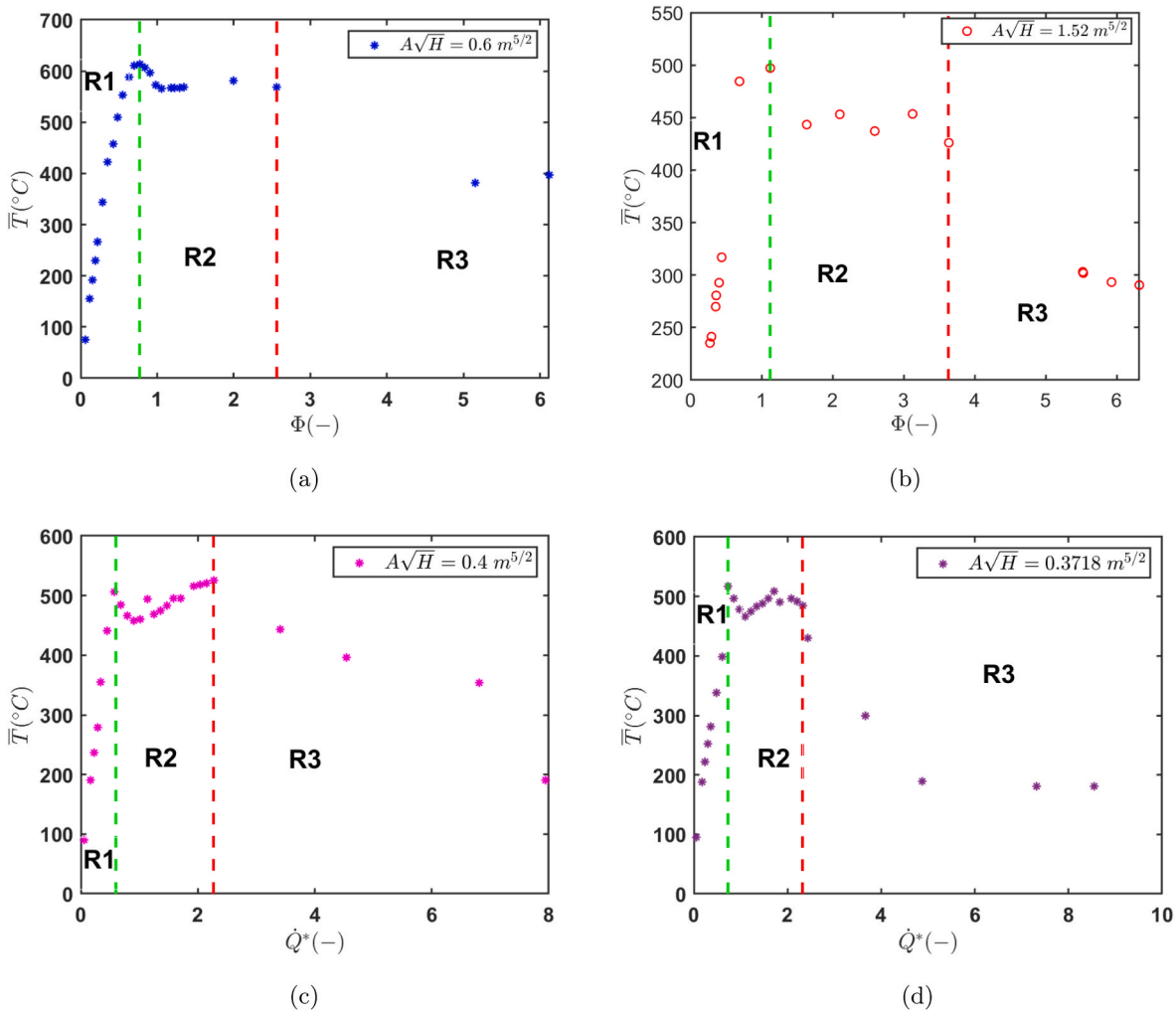

Fig. 9. (a) and (b) Average temperature inside the compartment versus the Global Equivalence Ratio, (c) and (d) Average temperature inside the compartment versus dimensionless heat release rate for different scales and ventilation factors, ∘ full-scale and * intermediate scale, the dashed lines mark the demarcation between the different regimes.

delimitation between the well-ventilated and the under-ventilated regimes using this technique. Fig. 10a shows the variation of the critical GER bounding the first and the second regime. This delimitation depends on the ventilation factor. For a ventilation factor less than 1 ($A\sqrt{H} < 1$) the critical GER varies in the range $0.6 < \Phi_{cri} < 1$. However, for ($A\sqrt{H} > 1$), the critical GER seems to be less scattered with an average value of $\Phi_{cri} = 1.1$.

Fig. 10b shows the variation of the second critical GER separating the second and the third regime, which also depends on the ventilation factor and varies between $\Phi = 1.5$ and $\Phi = 3.6$.

In a similar way, Fig. 11b shows the variation of the second critical dimensionless heat release rate delimiting the second and the third regime, also depending on the ventilation factor and varying between $\dot{Q}^*_{cri} = 2$ and $\dot{Q}^*_{cri} = 4.5$. It should be noted that these delimitations depend on the discretization of the considered HRR. In the present work, the relative uncertainty is estimated to be between 6 and 30%.

3.3. Effect of the extinction model

As it was mentioned in section 2, the extinction and, of course, the

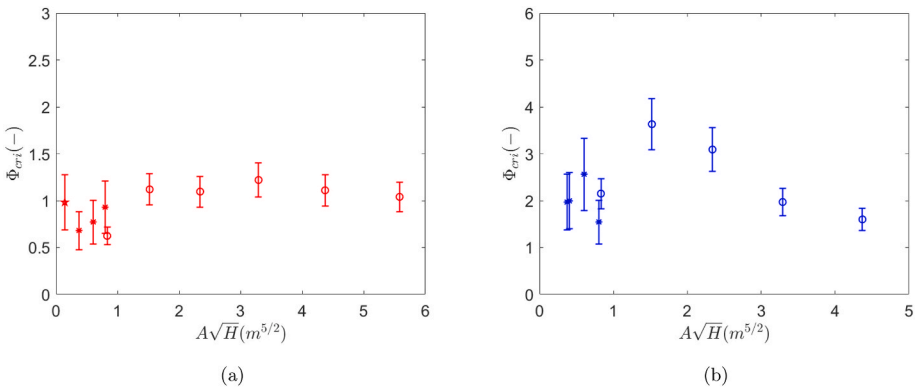

Fig. 10. Variation of the critical Global Equivalence Ratio marking the transition from the first to the second regime (a) and from the second to the third regime (b).

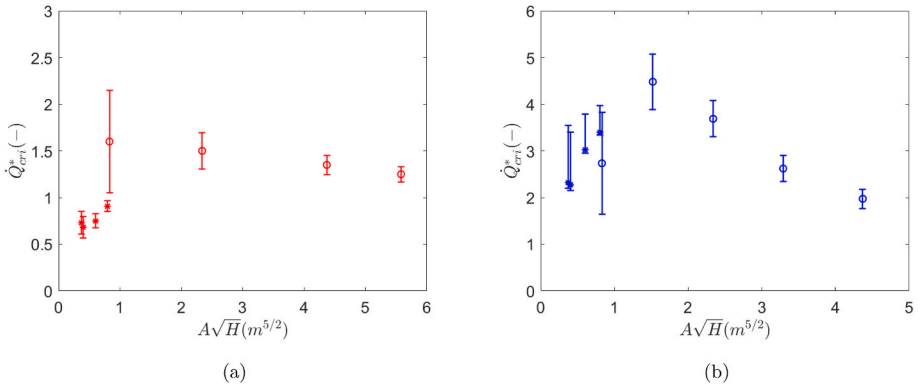

Fig. 11. Variation of the critical dimensionless heat release rate marking the transition from the first to the second regime (a) and from the second to the third regime (b).

transition from the well-ventilated to the under-ventilated regime, is highly dependent on the limiting oxygen fraction. In order to estimate this limiting fraction (Eq. (4)) the user needs to specify a critical flame temperature which can be highly dependent on the studied configuration. The choice of this temperature can be as important as the choice of the extinction model. As it was pointed out by Maragkos and Merci [40], in such model based on critical flame temperature, working with a constant value might be a weakness. For instance, as it was illustrated by Maragkos and Merci if we consider a laminar flame with a high residence time (time from initial temperature rise to the time of definite drop after reaching peak temperature) we could expect low critical flame temperature. But a flame with low residence times would lead to a high critical flame temperature. One solution is to consider an extinction model based on the Damköhler number $Da = (\tau_{mixixng}/\tau_{chemical})$, where $\tau_{mixixng}$ and $\tau_{chemical}$ are respectively the characteristic mixing and chemical time scales. A Damköhler number-based extinction model was implemented in FireFOAM by Vilfayeau [41] and evaluated against experimental work. A good agreement between the numerical and experimental results was observed.

In the present work, the extinction model has been modified in order to evaluate the effect of the limiting oxygen fraction on the combustion regimes. To evaluate the sensitivity of the simulations and the combustion regimes to the quenching model, we changed the extinction condition by setting the limiting oxygen fraction to zero ($Y^{lim}_{O_2} = 0$). Fig. 12 shows the variation of the ratio $\dot{Q}_{in}/P$ versus the Global Equivalence Ratio Φ. As it can be noticed, the critical GER ($\Phi_{cri} = 0.83$) delimiting the well-ventilated and under-ventilated regime predicted in this case ($Y^{lim}_{O_2} = 0$) is higher than the limit initially found ($\Phi_{cri} = 0.5$).

Once again, by analyzing the variation of the average temperature inside the compartment, two observations are drawn. First, changing the

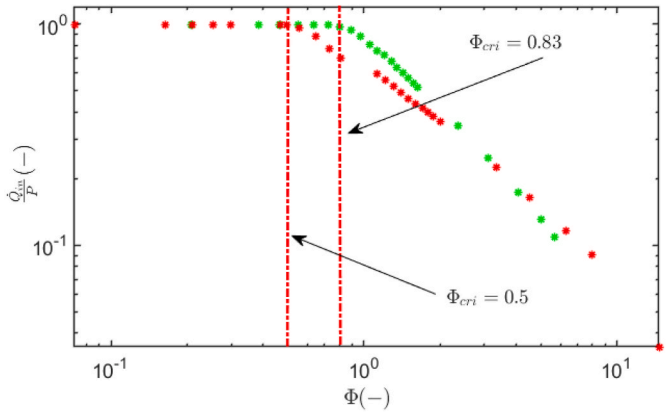

Fig. 12. Variation of the ratio $\frac{\dot{Q}_{in}}{P}$ versus the Global Equivalence Ratio for an intermediate scale with a ventilation factor of $A\sqrt{H} = 0.4\ m^{5/2}$ and a heat release rate 25 kW $\leq P \leq$ 3500 kW.

extinction limit allows to burn much more inside the enclosure. This increase in $\dot{Q}_{in}$ results in higher temperatures. The evolution of the average temperature inside the enclosure is represented in Fig. 13, where the green dots represent the simulations for which the extinction condition $Y^{lim}_{O_2}$ was set to zero and the red dots represent the simulations with the default settings. The second observation concerns the demarcation between the well-ventilated and under-ventilated regime. As it can be noticed in the case of the modified extinction condition, the critical GER ($\Phi_{cri} = 1.1$) is higher than the one predicted using the default parameters ($\Phi_{cri} = 0.65$). An equivalent analysis based on the

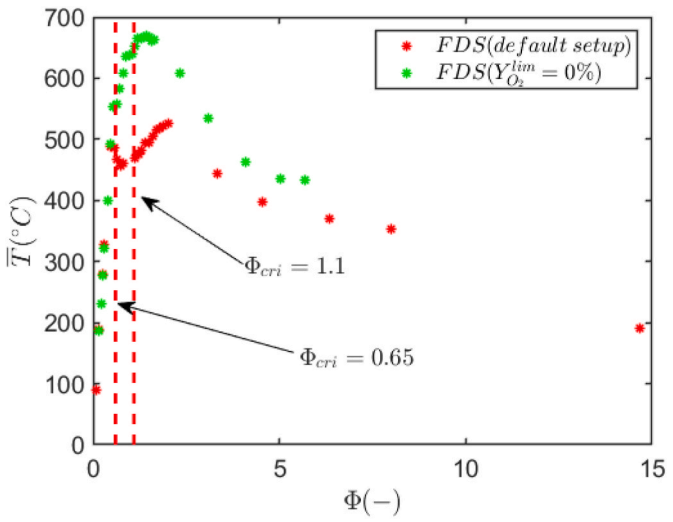

Fig. 13. Variation of the average temperature inside the compartment versus the Global Equivalence Ratio.

Table 2
Summary of the critical GER and dimensionless heat release rate obtained based on the variation of $\dot{Q}_{in}/P$ and the temperature T marking the transition between the first and second regimes. This demarcation is evaluated using both FDS default setup and modified version where the combustion limiting oxygen fraction was set to zero.

	FDS default		*FDS* ($Y_{O_2}^{lim}=0\%$)	
	$\dot{Q}_{in}/P$	T	$\dot{Q}_{in}/P$	T
Φ_{cri}	0.5	0.6–1.1	0.83	1.1
$\dot{Q}^*_{cri}$	0.6	0.4–1.6	0.9	1.5
$\dot{Q}^{cri}_{in}$	$660A\sqrt{H}$	$440-828\,A\sqrt{H}$	$991A\sqrt{H}$	$1238A\sqrt{H}$

dimensionless heat release rate was conducted and the results are summarized in Table 2. For both methods, the limitation determined based on the evolution of temperature is higher than the one obtained from the variation of the ratio $\dot{Q}_{in}/P$.

3.4. Variation of the maximum heat release rate inside the compartment

As it was pointed out earlier, the heat release rate inside a compartment can be estimated based on the amount of air entering though the opening. In general, this amount is expressed as a function of the ventilation factor $\dot{m}_{in} = 0.5\,A\sqrt{H}$. By assuming that all the air entering the compartment takes part in the reaction, the maximum heat release rate inside a compartment can be expressed as $\dot{Q}_{in}^{max} = 1500\,A\sqrt{H}(kW)$.

The heat release rate inside the compartment $\dot{Q}_{in}$ is evaluated by integrating the heat release rate over the domain (inside the compartment). For each configuration (a given ventilation factor $A\sqrt{H}$), the heat release rate inside the enclosure $\dot{Q}_{in}$ is evaluated for different prescribed heat release rates. Fig. 14a illustrates a typical evolution over time of the heat release rate inside the compartment ($\dot{Q}_{in}$)($A\sqrt{H}=0.4\ m^{5/2}$, $P=25$ kW). For each configuration (ventilation factor, prescribed heat release rate) the average value through the steady state is determined as illustrated by the red line in Fig. 14a. These mean values are presented in Fig. 14b as a function of the prescribed heat release rate P. This allowed us to determine the maximum heat release rate inside the compartment for each ventilation factor $A\sqrt{H}$, see Fig. 14c.

First, we can notice that there is a linear relationship between the $\dot{Q}_{in}$ and the ventilation factor $A\sqrt{H}$. However, the proportionality factor is different from the theoretical one, namely 850 instead of 1500. This difference is due to the fact that not all the oxygen entering the compartment is consumed during combustion and also to the difference in the inlet air flow: $\dot{m}_{in}^{max} = 0.46\,A\sqrt{H}$ numerically versus $\dot{m}_{in}^{max} = 0.5\,A\sqrt{H}$ theoretically. It should be noted that this value does not represent the transition between the well and the under-ventilated regimes. Indeed, based on the analysis of section 3.2, the transition takes place before reaching the maximum value of $\dot{Q}_{in}$.

4. Conclusion

A numerical investigation was performed for under-ventilated compartment fires, using the CFD code Fire Dynamics Simulator (FDS).

This work allowed us to determine a demarcation between the well-ventilated and the under-ventilated combustion regimes. This demarcation was obtained using two methods. The first one is based on the evaluation of the heat release rate inside the compartment and the second one is based on the analysis of the mean temperature.

For the first method, the demarcation between well-ventilated and under-ventilated regimes was obtained for a Global Equivalence Ratio $\Phi = 0.5$ or a dimensionless heat release rate $\dot{Q}^* = 0.6$. Based on the latter we can determine the heat release rate that can be reached inside the compartment before external flames appear. The second method is based on the temperature. This method can be useful in experimental studies since we do not have access to the heat release inside the compartment. The limit was observed for $0.6 < \Phi < 1.1$ or $0.4 < \dot{Q}^* < 1.6$. These limits can be converted to heat release rate, as it was summarized in Table 2.

Those limits highly depend on the extinction model. In order to evaluate its effects on the combustion regimes, the extinction criterion was modified by setting the limiting oxygen fraction to zero ($Y_{O_2}^{lim} = 0$). This change leads to the modification of the frontiers between the well-ventilated and the under-ventilated regime.

Concerning the transition from the regime 2 (combustion inside and outside the compartment) to regime 3 (most of the reaction takes place outside, which is characterized by a drop of the temperature inside the compartment) the critical Global Equivalence Ratio (Φ) and the dimensionless heat release rate $\dot{Q}^*$ vary over the ranges, $1.5 < \Phi < 3.6$ and $2 < \dot{Q}^* < 4.5$.

A linear relationship was found between the maximum heat release rate inside the compartment and the ventilation factor. The regression coefficient varies according to the extinction condition. We noted 850 in the case of the default setup and 1300 in the case of the extinction limit $Y_{O_2}^{lim} = 0$. Finally, the common linear relationship between the maximum inlet air flow and the ventilation factor ($\dot{m}_{in}^{max} = 0.46\,A\sqrt{H}$) was ascertained. These proportionality coefficients may vary depending on the used parameters, Table 3 gives a summary of the available numerical correlations.

This work will be followed by an experimental investigation, which will allow us to confirm this analysis and suggest some improvements if needed.

Author statement

Bouaza Lafdal: Conceptualization, Investigation, Methodology, Software, Writing - Original Draft, Writing - Review & Editing, Visualization.

Racha Djebbar: Conceptualization, Investigation, Methodology, Software, Writing - Original Draft, Writing - Review & Editing, Visualization.

Pascal Boulet: Conceptualization, Writing - Review & Editing, Supervision.

Rabah Mehaddi: Conceptualization, Methodology, Writing -

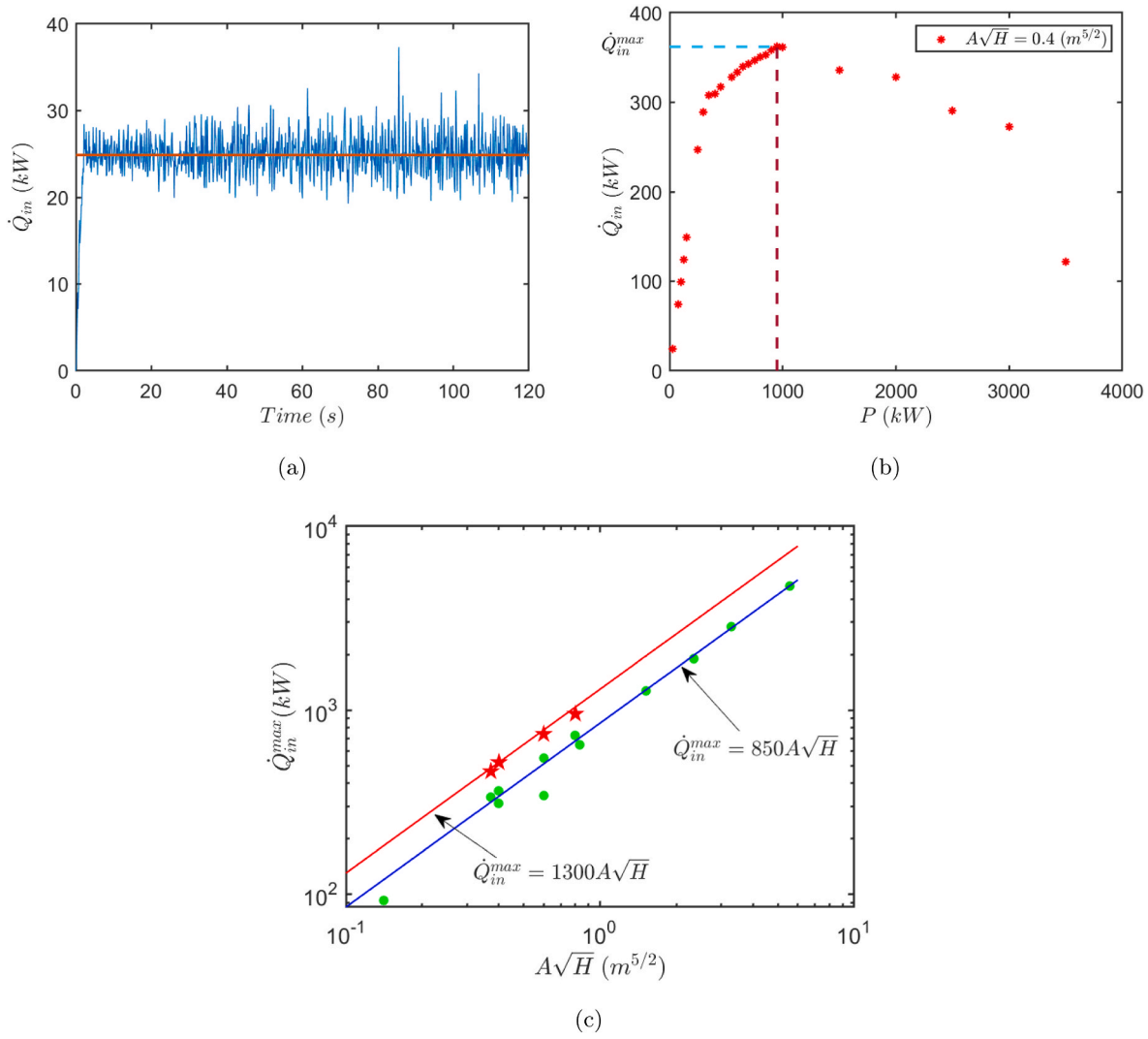

Fig. 14. (a) Evolution over time of the heat release rate inside the compartment ($\dot{Q}_{in}$)(intermediate scale, $A\sqrt{H} = 0.4\ m^{5/2}$, $P = 25$ kW), (b) variation of the $\dot{Q}_{in}$ average as a function of the prescribed heat release rate for a ventilation factor of 0.4 $m^{5/2}$, (c) variation of the maximum heat release rate inside the compartment ($\dot{Q}_{in}^{max}$) versus the ventilation factor. In (c), for the default setup all the simulations indicated in Table 1 were considered. However, for the modified version ($Y_{O_2}^{lim} = 0$), only the intermediate scale simulations were considered ($0.3718\ m^{5/2} \leq A\sqrt{H} \leq 0.8\ m^{5/2}$, 25 kW $\leq P \leq$ 3500 kW).

Table 3
Summary of the available numerical correlations in the literature.

Author	*CFD model*	*Parameters*	$\dot{Q}_{in}^{max} = K \times A\sqrt{H}$	$\dot{m}_{in}^{max} = C \times A\sqrt{H}$
Zhao et al [20]	*FDS* (6.0.1)	*Default Parameters*	$1130.7 \times A\sqrt{H}$	$0.41 \times A\sqrt{H}$
Asimakopoulou et al [21]	*FDS* (6.5.3)	*Default Parameters*	$950 \times A\sqrt{H}$	–
Cai and Chow [42]	*FDS* (*version* 5)	*Default Parameters*	–	$0.44 \times A\sqrt{H}$
Current study	*FDS* (6.7.0)	*Default Parameters*	$850 \times A\sqrt{H}$	$0.46 \times A\sqrt{H}$
Current study	*FDS* (6.7.0)	($Y_{O_2}^{lim} = 0\%$)	$1300 \times A\sqrt{H}$	$0.56 \times A\sqrt{H}$

Original Draft, Writing - Review & Editing, Visualization, Supervision.

El Mehdi Koutaiba: Conceptualization, Methodology, Writing - Review & Editing, Supervision.

Tarek Beji: Conceptualization, Methodology, Writing - Review & Editing, Supervision.

Jose Luis Torero: Conceptualization, Methodology, Writing - Review & Editing, Supervision.

Declaration of competing interest

The authors declare that they have no known competing financial interests or personal relationships that could have appeared to influence the work reported in this paper.

Acknowledgments

This work is conducted in the frame of a project of the joined research laboratory LEMTA/CSTB.

High Performance Computing resources were partially provided by the EXPLOR centre hosted by the University de Lorraine.

Appendix. A. Sensitivity analysis

In order to evaluate the mesh sensitivity, numerous simulations have been carried out where different mesh sizes have been used namely: 5 cm, 4 cm, 3 cm, 2 cm, 1.8 cm and 1.5 cm.

To assess the mesh convergence, we systematically measured the effect of the grid size on the temperature and velocity profiles at the door-way. As can be seen in Figure A.15, the temperature and velocity profiles start to be independent on the grid size for the mesh size of 2 cm. The maximum error between the 2 cm and the 1.5 cm mesh is about 2–4% for the temperature and 2–6% for the velocity.

In the same way, the convergence is also evaluated by the means of the temperature profiles recorded inside the compartment. Figure A.16 shows the velocity and temperature profiles inside the enclosure. Here again the mesh size of 2 cm seems to be the best compromise. These results emphasize and confirm the obtained estimation found in McGrattan et al. [33].

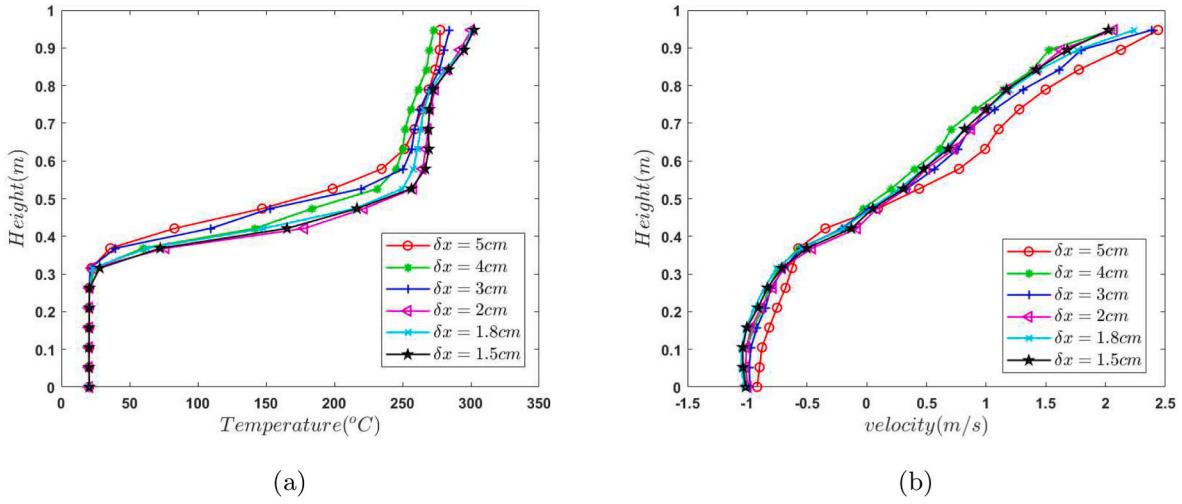

Fig. A.15. Temperature (a) and velocity (b) profiles at the door-way.

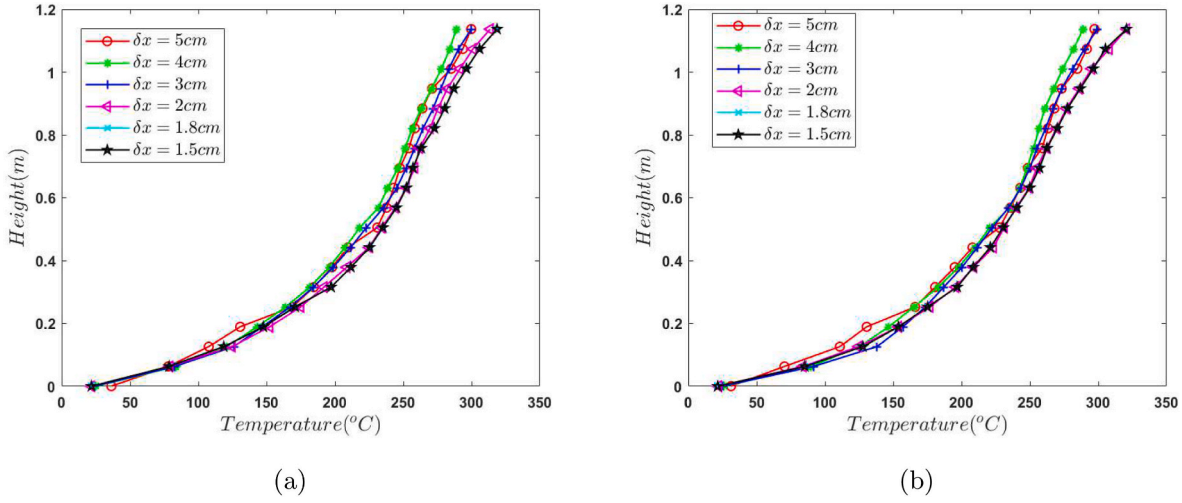

Fig. A.16. Temperature profiles inside the compartment at the position front right (a) and front left (b) (for the positions you may refer to the sketch in Fig. 2).

The domain extension beyond the compartment dimension is also a very important parameter and it has a significant influence on the simulation results [43]. If the external volume is too small, the influence on the different variables can be very important and if this extension is too large, the calculation time will increase significantly. As shown in Figure A.17 the variation of the velocity and temperature profiles at the opening are insensitive to the extension lengths (L) of 1 m, 2 m and 3 m. We can notice that the velocity and temperature profiles at the door-way are overlapped which means that extensions equal or larger than 1 m are sufficient to obtain accurate simulations. The same conclusion can be obtained by analyzing the temperature profiles inside the compartment represented in Figure A.18.

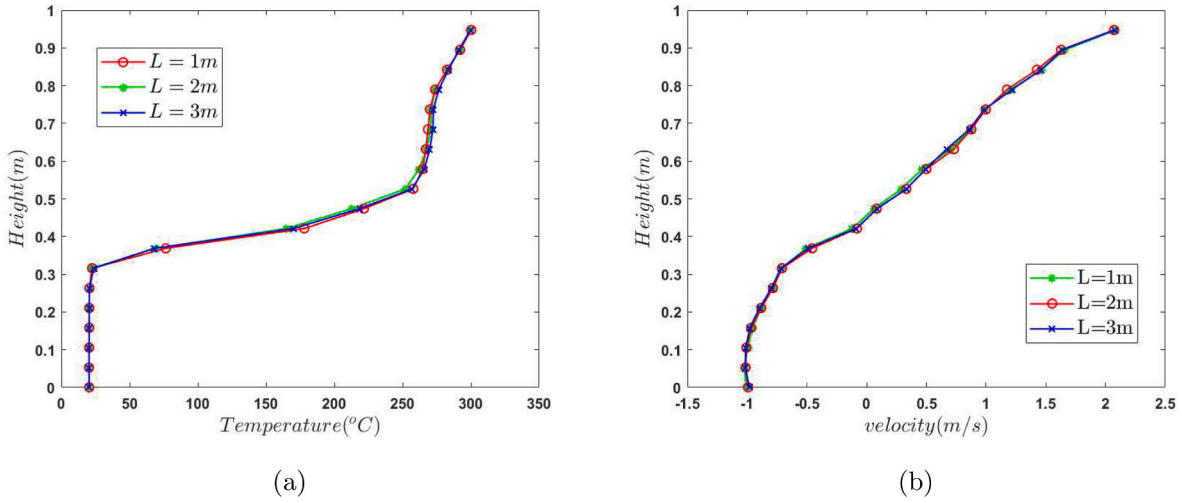

Fig. A.17. Temperature (a) and velocity (b) profiles at the door-way for different extension lengths (L).

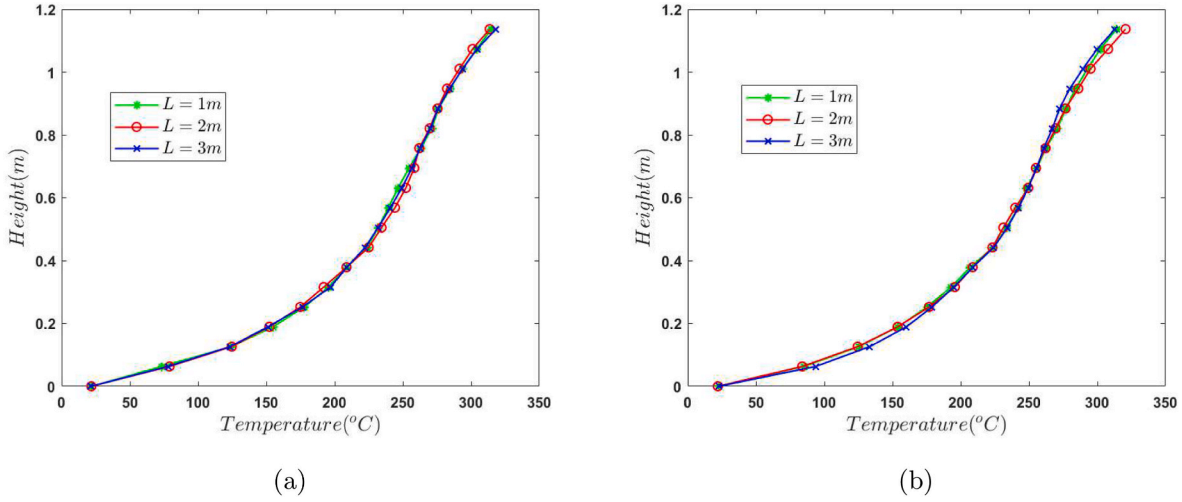

Fig. A.18. Temperature profiles inside the compartment at the position front right (a) and front left (b) (for the positions you may refer to the sketch in Fig. 2).

References

[1] K. Kawagoe, Fire behavior in rooms, in: Tech. Rep., 27, Building Research Institute, Ministry of Construction, Tokyo, 1958.

[2] V. Babrauskas, Estimating room flashover potential, Fire Technol. 16 (2) (1980) 94–103, https://doi.org/10.1007/BF02481843, 10.1007/BF02481843. URL.

[3] C. Huggett, Estimation of rate of heat release by means of oxygen consumption measurements, Fire Mater. 4 (2) (1980) 61–65, https://doi.org/10.1002/fam.810040202. URL, https://onlinelibrary.wiley.com/doi/10.1002/fam.810040202.

[4] B. Karlsson, J.G. Quintiere, Enclosure Fire Dynamics, 2000.

[5] J. Torero, A. Majdalani, C. Abecassis-Empis, A. Cowlard, Revisiting the compartment fire, Fire Saf. Sci. 11 (2014) 28–45, https://doi.org/10.3801/IAFSS.FSS.11-28. URL, http://www.iafss.org/publications/fss/11/28.

[6] A. H. Majdalani, Compartment Fire Analysis for Contemporary Architecture, University of Edinburgh. URL http://hdl.handle.net/1842/9969.

[7] H. Takeda, K. Akita, Critical phenomenon in compartment fires with liquid fuels, Symposium (International) on Combus. 18 (1) (1981) 519–527, https://doi.org/10.1016/S0082-0784(81)80057-4. URL, https://linkinghub.elsevier.com/retrieve/pii/S0082078481800574.

[8] A. Tewarson, Some observations on experimental fires in enclosures, Part II - Ethyl alcohol and paraffin Oil.pdf, Combust. Flame 19 (3) (1972) 363–371.

[9] K.I. Kim, H. Ohtani, Y. Uehara, Experimental study on oscillating behaviour in a small-scale compartment fire, Fire Saf. J. 20 (4) (1993) 377–384, https://doi.org/10.1016/0379-7112(93)90056-V. URL, https://linkinghub.elsevier.com/retrieve/pii/037971129390056V.

[10] Y. Utiskul, J.G. Quintiere, A.S. Rangwala, B.A. Ringwelski, K. Wakatsuki, T. Naruse, Compartment fire phenomena under limited ventilation, Fire Saf. J. 40 (4) (2005) 367–390, https://doi.org/10.1016/j.firesaf.2005.02.002. URL, https://linkinghub.elsevier.com/retrieve/pii/S0379711205000202.

[11] A.Y. Snegirev, G.M. Makhviladze, V.A. Talalov, A.V. Shamshin, Turbulent diffusion combustion under conditions of limited ventilation: flame projection through an opening, Combust. Explos. Shock Waves 39 (1) (2003) 1–10, https://doi.org/10.1023/A:1022189816023, doi:10.1023/A:1022189816023.

[12] A. Lock, G. Ko, M. Bundy, E. Johnsson, A. Hamins, Measurements in standard room scale fires, Fire Saf. Sci. 9 (2008) 873–882, https://doi.org/10.3801/IAFSS.FSS.9-873. URL, http://www.iafss.org/publications/fss/9/873.

[13] F. Ren, L. Hu, X. Zhang, X. Sun, J. Zhang, M. Delichatsios, Experimental study of transitional behavior of fully developed under-ventilated compartment fire and associated facade flame height evolution, Combust. Flame 208 (2019) 235–245, https://doi.org/10.1016/j.combustflame.2019.07.003. URL, https://linkinghub.elsevier.com/retrieve/pii/S0010218019302950.

[14] C. Heskestad, Modeling of enclosure fires, Symposium (International) on Combus. 14 (1) (1973) 1021–1030, https://doi.org/10.1016/S0082-0784(73)80092-X. URL, https://linkinghub.elsevier.com/retrieve/pii/S008207847380092X.
[15] J.G. Quintiere, Scaling applications in fire research, Fire Saf. J. 15 (1) (1989) 3–29, https://doi.org/10.1016/0379-7112(89)90045-3. URL, https://linkinghub.elsevier.com/retrieve/pii/0379711289900453.
[16] J. Quintiere, B.J. McCAFFREY, T. Kashiwagi, A scaling study of a corridor subject to a room fire, Combust. Sci. Technol. 18 (1–2) (1978) 1–19, https://doi.org/10.1080/00102207808946835. URL, http://www.tandfonline.com/doi/abs/10.1080/00102207808946835.
[17] J.G. Quintiere, Fundamentals of Fire Phenomena, Wiley, Chichester, 2006, p. 254253146, oCLC.
[18] R.I. Emori, K. Saito, A study of scaling laws in pool and crib fires, Combust. Sci. Technol. 31 (5–6) (1983) 217–231, https://doi.org/10.1080/00102208308923643. URL, http://www.tandfonline.com/doi/abs/10.1080/00102208308923643.
[19] S. Suard, A. Koched, H. Pretrel, L. Audouin, Numerical simulations of fire-induced doorway flows in a small scale enclosure, Int. J. Heat Mass Tran. 81 (2015) 578–590, https://doi.org/10.1016/j.ijheatmasstransfer.2014.10.069. URL, https://linkinghub.elsevier.com/retrieve/pii/S001793101400965X.
[20] G. Zhao, T. Beji, B. Merci, Application of FDS to under-ventilated enclosure fires with external flaming, Fire Technol. 52 (6) (2016) 2117–2142, https://doi.org/10.1007/s10694-015-0552-4. URL, http://link.springer.com/10.1007/s10694-015-0552-4.
[21] A. Afflard, E. M. Koutaiba, E. Asimakopoulou, D. Kolaitis, J. Zhang, Numerical investigation of fire development in a medium scale iso9705 compartment-façade configuration, Int. Sympos. Fire Saf. Facades 9. URL https://www.researchgate.net/publication/336318842.
[22] X. Sun, L. Hu, X. Zhang, Y. Yang, F. Ren, X. Fang, K. Wang, H. Lu, Temperature evolution and external flame height through the opening of fire compartment: scale effect on heat/mass transfer and revisited models, Int. J. Therm. Sci. 164 (2021) 106849, https://doi.org/10.1016/j.ijthermalsci.2021.106849. URL, https://linkinghub.elsevier.com/retrieve/pii/S1290072921000193.
[23] https://www.nist.gov/services-resources/software/fds-and-smokeview.
[24] K. McGrattan, S. Hostikka, J. Floyd, R. McDermott, M. Vanella, Fire dynamics simulator (version 4), technical reference guide, in: Tech. Rep. NIST SP 1018, edition, National Institute of Standards and Technology, Gaithersburg, MD, 2006, https://doi.org/10.6028/NIST.SP.1018. URL, https://nvlpubs.nist.gov/nistpubs/Legacy/SP/nistspecialpublication1018.pdf.
[25] K. McGrattan, S. Hostikka, J. Floyd, R. McDermott, M. Vanella, Fire dynamics simulator (version 4), technical reference guide, volume 3: validation, in: Tech. Rep. NIST SP 1018, edition, National Institute of Standards and Technology, Gaithersburg, MD, 2006, https://doi.org/10.6028/NIST.SP.1018. URL, https://nvlpubs.nist.gov/nistpubs/Legacy/SP/nistspecialpublication1018.pdf.
[26] C.-H. Hwang, A. Lock, M. Bundy, E. Johnsson, Gwon Hyun Ko, Studies on fire characteristics in over- and underventilated full-scale compartments, J. Fire Sci. 28 (5) (2010) 459–486, https://doi.org/10.1177/0734904110363106. URL, http://journals.sagepub.com/doi/10.1177/0734904110363106.
[27] A. Lock, M. Bundy, E.L. Johnsson, A. Hamins, G.H. Ko, C. Hwang, P. Fuss, R. H. Harris, Experimental study of the effects of fuel type, fuel distribution and vent size on full-scale underventilated compartment fires in an ISO 9705 room, in: Tech. Rep. NIST TN 1603, edition, National Institute of Standards and Technology, Gaithersburg, MD, 2008, https://doi.org/10.6028/NIST.TN.1603. URL, https://nvlpubs.nist.gov/nistpubs/Legacy/TN/nbstechnicalnote1603.pdf.
[28] D. Pikiokos, Numerical simulation of compartment fires: investigation of opening flow characteristics Publisher: National Technological University of Athens, URL, https://dspace.lib.ntua.gr/xmlui/handle/123456789/43165.
[29] R.A. Bryant, A comparison of gas velocity measurements in a full-scale enclosure fire, Fire Saf. J. 44 (5) (2009) 793–800, https://doi.org/10.1016/j.firesaf.2009.03.010. URL, https://linkinghub.elsevier.com/retrieve/pii/S0379711209000447.
[30] R.A. Bryant, Evaluating practical measurements of fire-induced vent flows with stereoscopic PIV, Proc. Combust. Inst. 33 (2) (2011) 2481–2487, https://doi.org/10.1016/j.proci.2010.06.105. URL, https://linkinghub.elsevier.com/retrieve/pii/S1540748910001835.
[31] R.A. Bryant, The application of stereoscopic PIV to measure the flow of air into an enclosure containing a fire, Exp. Fluid 47 (2) (2009) 295–308, https://doi.org/10.1007/s00348-009-0656-z. URL, http://link.springer.com/10.1007/s00348-009-0656-z.
[32] K.A. Moinuddin, J.S. Al-Menhali, K. Prasannan, I.R. Thomas, Rise in structural steel temperatures during ISO 9705 room fires, Fire Saf. J. 46 (8) (2011) 480–496, https://doi.org/10.1016/j.firesaf.2011.08.001. URL, https://linkinghub.elsevier.com/retrieve/pii/S0379711211001093.
[33] K. McGrattan, H. Baum, R. Rehm, Large eddy simulations of smoke movement, Fire Saf. J. 30 (2) (1998) 161–178, https://doi.org/10.1016/S0379-7112(97)00041-6. URL, https://linkinghub.elsevier.com/retrieve/pii/S0379711297000416.
[34] B. Merci, K. Van Maele, Numerical simulations of full-scale enclosure fires in a small compartment with natural roof ventilation, Fire Saf. J. 43 (7) (2008) 495–511, https://doi.org/10.1016/j.firesaf.2007.12.003. URL, https://linkinghub.elsevier.com/retrieve/pii/S0379711207001294.
[35] K.B. McGrattan, G.P. Forney, Fire dynamics simulator (version 4) :: user's guide, in: Tech. Rep. NIST SP 1019, National Institute of Standards and Technology, Gaithersburg, MD, 2004, https://doi.org/10.6028/NIST.SP.1019. URL, https://nvlpubs.nist.gov/nistpubs/Legacy/SP/nistspecialpublication1019.pdf.
[36] M.A. Delichatsios, G.W. Silcock, X. Liu, M. Delichatsios, Y.-P. Lee, Mass pyrolysis rates and excess pyrolysate in fully developed enclosure fires, Fire Saf. J. 39 (1) (2004) 1–21, https://doi.org/10.1016/j.firesaf.2003.07.006. URL, https://linkinghub.elsevier.com/retrieve/pii/S0379711203000985.
[37] V. Babrauskas, W.J. Parker, G. Mulholland, W.H. Twilley, The Phi Meter: A Simple, Fuelindependent Instrument for Monitoring Combustion Equivalence Ratio, 1994, https://doi.org/10.1063/1.1144690, 10doi:10.1063/1.1144690. URL.
[38] W.M. Pith, The Global Equivalence Ratio Concept and the Formation Mechanisms of Carbon Monoxide in Enclosure Fires, 1995, p. 41, https://doi.org/10.1016/0360-1285(95)00004-2.
[39] E. Zukoski, Fluid dynamic aspects of room fires, Fire Saf. Sci. 1 (1986) 1–30, https://doi.org/10.3801/IAFSS.FSS.1-1. URL, http://www.iafss.org/publications/fss/1/1.
[40] G. Maragkos, B. Merci, Large eddy simulations of flame extinction in a turbulent line burner, Fire Saf. J. 105 (2019) 216–226, https://doi.org/10.1016/j.firesaf.2019.03.008. URL, https://linkinghub.elsevier.com/retrieve/pii/S0379711218305630.
[41] S. Vilfayeau, Large Eddy Simulation of Fire Extinction Phenomena, Ph.D. thesis, University of Maryland, College Park, 2015.
[42] N. Cai, W.K. Chow, Numerical studies on heat release rate in room fire on liquid fuel under different ventilation factors, Int. J. Chem. Eng. 2012 (2012) 1–13, https://doi.org/10.1155/2012/910869. URL, http://www.hindawi.com/journals/ijce/2012/910869/.
[43] Y. He, C. Jamieson, A. Jeary, J. Wang, Effect of computation domain on simulation of small compartment fires, Fire Saf. Sci. 9 (2008) 1365–1376, https://doi.org/10.3801/IAFSS.FSS.9-1365. URL, http://www.iafss.org/publications/fss/9/1365.